# Input-output system identification of a thermoacoustic oscillator near a Hopf bifurcation using only fixed-point data

Minwoo Lee,[1] Yu Guan,[1] Vikrant Gupta,[2,*] and Larry K. B. Li[1,†]

[1]*Department of Mechanical and Aerospace Engineering, The Hong Kong University of Science and Technology, Clear Water Bay, Hong Kong*

[2]*Department of Mechanics and Aerospace Engineering, Southern University of Science and Technology, Shenzhen, China*

(Received 5 October 2019; published 6 January 2020)

We present a framework for performing input-output system identification near a Hopf bifurcation using data from only the fixed-point branch, prior to the Hopf point itself. The framework models the system with a van der Pol–type equation perturbed by additive noise, and identifies the system parameters via the corresponding Fokker-Planck equation. We demonstrate the framework on a prototypical thermoacoustic oscillator (a flame-driven Rijke tube) undergoing a supercritical Hopf bifurcation. We find that the framework can accurately predict the properties of the Hopf bifurcation and the limit cycle beyond it. This study constitutes an experimental demonstration of system identification on a reacting flow using only prebifurcation data, opening up pathways to the development of early warning indicators for nonlinear dynamical systems near a Hopf bifurcation.

DOI: 10.1103/PhysRevE.101.013102

## I. INTRODUCTION

Many natural and engineered systems are nonlinear and can develop self-sustained oscillations [1]. Such oscillations are desirable in some systems (e.g., musical instruments [2], pendulum clocks [3], and pulsed combustors [4]) but they are undesirable in other systems (e.g., bridge structures [5], predator-prey systems [6], and gas turbines [7]). A canonical way for self-sustained oscillations to arise is via a Hopf bifurcation [1], in which a fixed point loses stability and a complex conjugate pair of eigenvalues crosses the imaginary axis in response to changes in a control parameter [8]. The result is a transition from a fixed point to a limit cycle [8]. If the limit cycle arises only after the Hopf point and its amplitude increases gradually with changes in the control parameter, then the Hopf bifurcation is supercritical. If the limit cycle arises in a hysteric bistable regime, between the Hopf and saddle-node points, and its amplitude increases abruptly, then the Hopf bifurcation is subcritical. Whether a Hopf bifurcation is supercritical or subcritical depends on the specific form of nonlinearity in the system [8]. In many practical systems, it is advantageous to be able to predict the type and location of the Hopf bifurcation, because this can enable users to avoid destructive acoustic or structural resonances. Thus there is a need for robust methods capable of identifying the nonlinear properties of dynamical systems using only prebifurcation data. In this paper, we demonstrate a framework for this that uses the noise-perturbed data on the fixed-point branch, prior to the Hopf point itself.

### A. Thermoacoustic instability via a Hopf bifurcation

Despite significant research, thermoacoustic instability continues to hamper the development of combustion devices such as gas turbines and rocket engines [9,10]. The underlying cause of this instability is the positive feedback between the heat-release-rate (HRR) oscillations of an unsteady flame and the pressure oscillations of its surrounding combustor [11]. If the HRR oscillations are sufficiently in phase with the pressure oscillations, the former can transfer energy to the latter via the Rayleigh mechanism [12], leading to self-sustained flow oscillations at one or more of the natural acoustic modes of the system [13,14]. If severe, such thermoacoustic oscillations can exacerbate vibration, mechanical fatigue, and thermal loading, reducing the reliability of the overall system. This problem is especially concerning in modern gas turbines because the conditions under which such devices must operate to achieve low pollutant emissions are also those that provoke thermoacoustic instability [7].

Like other self-sustained oscillations, thermoacoustic oscillations often arise via a Hopf bifurcation, making them amenable to a weakly nonlinear analysis near the Hopf point [15]. Such an analysis can be performed with the normal-form equation for a Hopf bifurcation, which, in fluid mechanics, is known as the Stuart-Landau equation [16]:

$$\frac{da}{dt} = k_1 a + k_2 a^3 + \cdots , \tag{1}$$

where $a$ is the complex mode amplitude, $k_1$ is the linear driving or damping coefficient, $k_2$ is a nonlinear coefficient, and $t$ is time. A Hopf bifurcation occurs at $k_1 = 0$. The Stuart-Landau equation can capture the amplitude evolution of a system near the Hopf point, where the growth rate, which controls the amplitude evolution, is still much smaller than the oscillation frequency. Weakly nonlinear analyses based on the Stuart-Landau equation have been used before to study hydrodynamic systems [17–21] and thermoacoustic systems [22,23]. For example, Orchini *et al.* [24] recently carried out a weakly nonlinear analysis of a Rijke tube and showed that such an approach can reduce the computational cost of investigating oscillatory phenomena near a Hopf bifurcation.

*vik.gupta@cantab.net
†larryli@ust.hk

 

### B. Noise-induced dynamics of thermoacoustic systems

Thermoacoustic systems often exhibit combustion noise, which can arise from direct sources, such as the HRR fluctuations of an unsteady flame, and indirect sources, such as the acceleration of entropy or vortical inhomogeneities through a nozzle [25]. Previous studies on the noise-induced dynamics of thermoacoustic systems have focused primarily on two objectives: (i) to investigate the dynamical effect of noise, such as how it shifts the stability boundaries [26,27] and how it triggers limit-cycle oscillations in the bistable regime [28,29], and (ii) to gather information about the system from its noise-induced dynamics. Such information can then be used to predict the onset of instability [30–36], to distinguish between supercritical and subcritical bifurcations [37], and to extract deterministic quantities [38–41].

The noise-induced dynamics of a system can be determined by measuring its response to extrinsic or intrinsic perturbations [42]. In the early years of rocket development, extrinsic perturbations in the form of bomb detonations were used in combustors to determine their stochastic properties and stability boundaries [43]. In recent years, such noise-induced dynamics has been used to forecast the onset of thermoacoustic instability. For example, Kabiraj *et al.* [30] applied extrinsic perturbations to a thermoacoustic system and found that its degree of coherence peaks at an intermediate noise amplitude—a phenomenon called coherence resonance. These researchers noted that such dynamics could be used as a precursor to a Hopf bifurcation. Other metrics capable of forecasting the onset of thermoacoustic instability include the Hurst exponent [32], ordinal partition transition networks [33], the phase parameter [34], sequential horizontal-visibility-graph motifs [35], and the autocorrelation function and variance [36]. In the present study, we build on these contributions by showing that it is possible to predict the properties of a Hopf bifurcation and the resultant limit cycle, using only prebifurcation data and without the need to set *ad hoc* instability thresholds.

### C. System identification

System identification (SI) refers to the use of statistical methods to construct mathematical models of dynamical systems from input and/or output data. There are two main ways in which SI can be performed: data-driven SI and model-based SI. In data-driven SI, *a priori* knowledge of the system physics is not required. Instead, a model of the system is found solely from data using techniques such as symbolic regression [44] and machine learning [45]. Data-driven SI is useful when abundant data are available, either from experiments or simulations. However, in practical systems, it is often difficult and costly to acquire sufficient data. In such cases, it may be more efficient to use model-based SI, in which a low-dimensional model is assumed or developed for a system using information about its physics, and then the coefficients of the model are determined from data [46].

In thermoacoustics, most studies relying on the noise-induced dynamics for SI have used a model-based approach [9,47]. For example, Noiray's group used a self-sustained oscillator equation perturbed by additive noise to model the dynamics of a gas-turbine combustor perturbed by its own turbulence [38–41]. Specifically, Noiray and Schuermans [38] used stochastic differential equations, based on the Fokker-Planck formalism, to extract deterministic quantities from noise-perturbed data. Recently, Boujo and Noiray [40] improved the accuracy of this SI method by incorporating adjoint-based optimization. In these studies [38–41], an intrinsic noise source, namely turbulence, was used to extract the system coefficients. This output-only approach is convenient in that neither an actuator model nor extrinsic forcing is required. However, like most SI methods, it requires at least some data from the limit-cycle branch. By contrast, Lee *et al.* [48] recently proposed an input-output SI framework in which extrinsic noise is fed into the system to enable prediction of its bifurcation properties and limit-cycle amplitudes, using data from only the fixed-point branch, before the Hopf point itself. To date, however, the SI framework of Lee *et al.* [48] has only been demonstrated on a simple hydrodynamic system, a low-density jet, which has none of the complexities of a thermoacoustic system such as nonlinear coupling between HRR oscillations and sound waves.

### D. Contributions of the present study

In this study, we apply the SI framework of Lee *et al.* [48] to a prototypical thermoacoustic system, a flame-driven Rijke tube, undergoing a supercritical Hopf bifurcation. We show that this framework can enable accurate prediction of the properties of the Hopf bifurcation and the limit cycle beyond it, using nothing more than the noise-perturbed data on the fixed-point branch, prior to the Hopf point itself. Crucially, we show that, unlike most other forecasting methods, ours does not require empirical instability thresholds to be set *ad hoc*, implying that our method can give objective predictions for a variety of nonlinear dynamical systems. Below we present the experimental setup (Sec. II), review the SI framework of Lee *et al.* [48] (Sec. III), and apply that framework to a thermoacoustic system (Sec. IV), before concluding with the key implications and limitations of this study (Sec. V).

## II. EXPERIMENTAL SETUP

The thermoacoustic system under study consists of a vertical tube combustor containing a laminar conical premixed flame. This system, which is also known as a flame-driven Rijke tube, can exhibit a variety of nonlinear states and bifurcations, making it an ideal platform for studying thermoacoustic phenomena [49–52]. Shown in Fig. 1, the system features a stainless-steel tube burner [inner diameter (ID) = 16.8 mm; length = 800 mm], a double-open-ended quartz tube combustor (ID = 44 mm; length $L$ = 860 mm), and an acoustic decoupler (ID = 180 mm; length = 200 mm). The flame is stabilized on a copper extension tip (ID: $D$ = 12 mm; length = 30 mm) mounted at the burner outlet. Extrinsic perturbations are applied to the system via a loudspeaker (FaitalPRO 6FE100) mounted in the acoustic decoupler. The loudspeaker is driven by a white Gaussian noise signal from a function generator (Keysight 33512B) via a power amplifier (Alesis RA150). The fuel used for the flame is liquefied petroleum gas (70% butane, 30% propane). The fuel flow rate is controlled with a rotameter (±2.5%) and the air flow

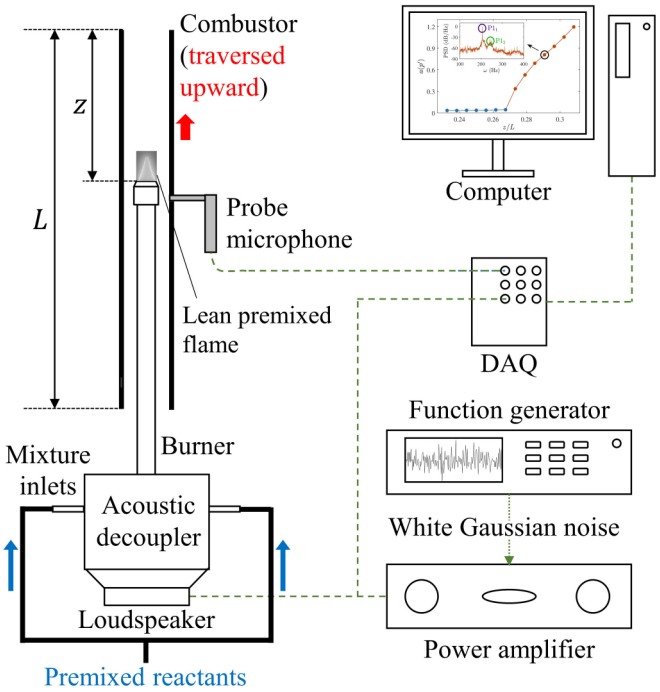


FIG. 1. Schematic of the experimental setup consisting of a prototypical thermoacoustic system (a flame-driven Rijke tube) perturbed by extrinsic noise from a loudspeaker. DAQ: data acquisition system.

rate is controlled with a mass flow controller (Alicat MCR: ±0.2%). In this study, the system is operated at an equivalence ratio of 0.62 (±3.2%), a bulk reactant velocity of $\bar{u} = 1.6$ m/s (±0.2%), and a Reynolds number of Re = 1300 (±1.7%) based on $\bar{u}$ and $D$.

To induce a Hopf bifurcation, we traverse the combustor upward relative to the stationary burner. The nondimensional flame position ($z/L$) is defined as the distance from the top of the combustor to the burner extension tip ($z$) normalized by the combustor length ($L$). To determine the state of the system, we use the acoustic pressure fluctuation ($p'$), which is measured with a probe microphone (GRAS 40SA, $\pm 2.5 \times 10^{-5}$ Pa sensitivity) mounted 387 mm from the bottom of the combustor. For each test run, we collect 8 s long time traces of $p'$ at a sampling frequency of 32768 Hz, which is more than 150 times the frequency of the incipient limit cycle.

## III. SYSTEM-IDENTIFICATION FRAMEWORK

As mentioned in Sec. I, we use the input-output SI framework developed in our previous study [48]. A detailed description of this framework can be found in that study [48], so only a brief overview is given below.

### A. System model

To model the thermoacoustic system, we use a high-order Duffing–van der Pol (DVDP) oscillator perturbed by additive white Gaussian noise [48]:

$$\ddot{x} - (\epsilon + \alpha_1 x^2 + \alpha_2 x^4 + \alpha_3 x^6 + \cdots)\dot{x} + x + \beta x^3 = \sqrt{2d}\,\eta(t), \tag{2}$$

where $x$ represents the pressure fluctuation in the combustor ($p'$ in units of Pa), $\eta(t)$ is a unit noise term, $d$ is the noise amplitude, $\epsilon$ is the linear growth (positive) or damping (negative) term, $\alpha_1, \alpha_2, \alpha_3, \ldots$ are the nonlinear terms, and $\beta$ is the anisochronicity factor, which determines the frequency shift as a function of amplitude. The point at which $\epsilon$ crosses zero is the Hopf point, with the sign of $\alpha_1$ determining whether the Hopf bifurcation is supercritical (negative) or subcritical (positive).

The probabilistic solution to Eq. (2) can be found via the method of variation of parameters [53]. On substitution of $x$ and $\dot{x}$ as $x(t) = a(t)\cos[t + \phi(t)]$ and $\dot{x}(t) = -a(t)\sin[t + \phi(t)]$, we obtain two first-order equations for the amplitude ($a$) and the phase ($\phi$):

$$\dot{a} = \left(\frac{\epsilon}{2}a + \frac{\alpha_1}{8}a^3 + \frac{\alpha_2}{16}a^5 + \frac{5\alpha_3}{128}a^7 + \cdots\right) + Q_1(a, \Phi) - (\sqrt{2d}\,\sin\Phi)\eta, \tag{3a}$$

$$\dot{\phi} = \frac{3\beta}{8}a^2 + Q_2(a, \Phi) - \left(\frac{\sqrt{2d}}{a}\cos\Phi\right)\eta, \tag{3b}$$

where $\eta$ is a unit white Gaussian noise term, $\Phi(t) = t + \phi(t)$, and $Q_1(a, \Phi)$ and $Q_2(a, \Phi)$ are the sum of all the terms with first-order sine and cosine terms. Assuming that $a$ and $\phi$ vary much more slowly than $x$ itself, we can justifiably neglect $Q_1(a, \Phi)$ and $Q_2(a, \Phi)$ via time averaging [53]. Thus, for zero noise ($d = 0$), Eq. (3a) can be rewritten as

$$\frac{da}{dt} = \frac{\epsilon}{2}a + \frac{\alpha_1}{8}a^3 + \frac{\alpha_2}{16}a^5 + \frac{5\alpha_3}{128}a^7 + \cdots. \tag{4}$$

Equation (4) takes the form of a Stuart-Landau equation, which is often used to model fluid-mechanical systems near a Hopf bifurcation [17,20,21,38,40,48,54,55]. This equation will later be used to calculate the noise-free bifurcation diagram. However, if the noise amplitude is finite ($d > 0$), stochastic averaging can be applied to Eq. (3), yielding the following stochastic differential equation, expressed here in Itô sense [42,56]:

$$da = \underbrace{\left(\frac{d}{2a} + \frac{\epsilon}{2}a + \frac{\alpha_1}{8}a^3 + \frac{\alpha_2}{16}a^5 + \frac{5\alpha_3}{128}a^7 + \cdots\right)}_{m(a,t)} dt + \underbrace{(\sqrt{d})}_{\sigma(a,t)} dW, \tag{5}$$

where $dW$ is a unit Wiener process and $m(a, t)$ and $\sigma(a, t)$ appear in the drift and diffusion terms of $a$, respectively. These two terms can be used to derive the classic Fokker-Planck equation:

$$\frac{\partial}{\partial t}P(a, t) = -\frac{\partial}{\partial a}[\boldsymbol{m}(a, t)P(a, t)] + \frac{\partial[}{\partial 2}]a\left[\frac{\boldsymbol{\sigma}^2(a, t)}{2}P(a, t)\right], \tag{6}$$

where $P(a, t)$ is the probability density function at time $t$. The stationary probability density function, $P(a)$, is found by

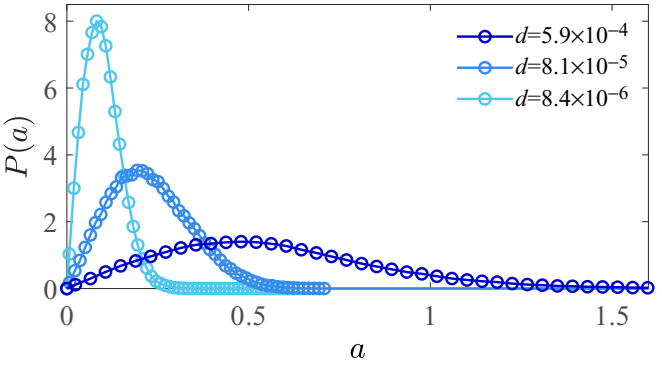


FIG. 2. Probability density function of the pressure fluctuation amplitude on the fixed-point branch ($z/L = 0.256$) for three different noise amplitudes ($d$).

integrating Eq. (6):

$$P(a) = Ca\,\exp\left[\frac{a^2}{d}\left(\frac{\epsilon}{2} + \frac{\alpha_1}{16}a^2 + \frac{\alpha_2}{48}a^4 + \frac{5\alpha_3}{512}a^6 + \cdots\right)\right], \tag{7}$$

where $C$ is a normalization constant and $P(a)$ is independent of the anisochronicity factor $\beta$ [57].

### B. System identification

We perform SI using probability density functions of the pressure fluctuation amplitude on the fixed-point branch, a subset of which is shown in Fig. 2. By taking the logarithm of Eq. (7), we obtain

$$\ln P(a) - \ln a = \ln C + \frac{\epsilon}{2d}a^2 + \frac{\alpha_1}{16d}a^4 + \frac{\alpha_2}{48d}a^6 + \cdots. \tag{8}$$

The left-hand side of Eq. (8) is measured experimentally for a given value of $a$. Thus the ratio of $d$ to the unknown coefficients on the right-hand side ($\epsilon/2d, \alpha_1/16d, \ldots$) can be extracted via polynomial regression. The number of terms on the right-hand side, which defines the order of nonlinearity, is determined by incrementally adding higher-order terms until the rank of the polynomial regression becomes deficient.

At each flame position ($z/L$), 16 different noise amplitudes ($d$) are applied, with three replications performed at each $d$. The system coefficients at each $z/L$ are then found by averaging the results across all values of $d$.

### C. Actuator model

A key component of input-output SI is the actuator model, which here is a function that transforms the loudspeaker voltage ($V$) into input noise ($d$). We use a power-law relationship for the actuator model, $d = b + kV^n$, where $b$ is the background noise amplitude and $k$ and $n$ are constants. Assuming $b \ll d$, we take the logarithm of this power-law equation, yielding

$$\ln\left(\frac{d}{c}\right) \approx n\,\ln V + \ln\left(\frac{k}{c}\right), \tag{9}$$

where $c$ is an arbitrary constant. From Sec. III B, a ratio between $d$ and one of the system parameters ($\epsilon, \alpha_1, \alpha_2, \ldots$) can be found before applying the actuator model. Thus, by replacing $c$ with one of those parameters, $n$ can be found from linear regression [Fig. 3(a)]. In this study, $|\epsilon|$ on the fixed-point branch is chosen because its values, sampled over multiple experimental runs, are the most consistent among all the DVDP coefficients. To find the remaining constants ($k$ and $b$), we use information in the spectral domain, as per Ushakov *et al.* [58]:

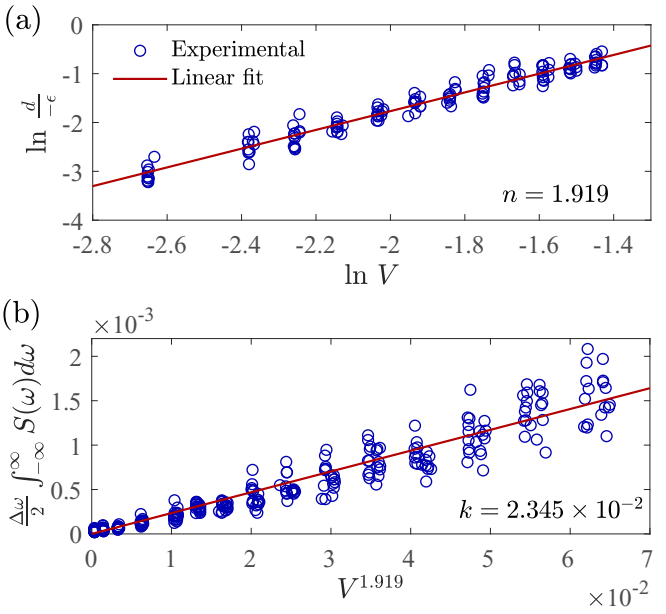


FIG. 3. Identification of the actuator model coefficients, where $n$ is the gradient of subfigure (a) and $k$ is the gradient of subfigure (b). The vertical intercept of subfigure (b) is the background noise amplitude ($b$), which is negligible and thus consistent with our modeling assumptions.

$$d = b + kV^n = \frac{\Delta\omega}{2}\int_{-\infty}^{\infty} S_u(\omega)d\omega, \tag{10}$$

where $S_u$ is the spectrum and $\Delta\omega$ is the half width at half maximum of a Lorentzian fit to the noise-induced peak in the power spectral density (PSD), as shown in Fig. 4. Finally, $k$

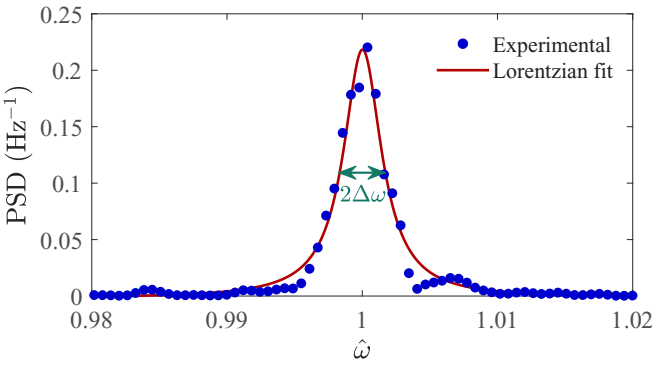


FIG. 4. Power spectral density showing a noise-induced peak and its Lorentzian fit on the fixed-point branch ($z/L = 0.267$) for $d = 4.0 \times 10^{-4}$. The horizontal axis is the normalized frequency ($\hat{\omega}$), with $2\Delta\omega$ denoting the width at half maximum of the Lorentzian fit.

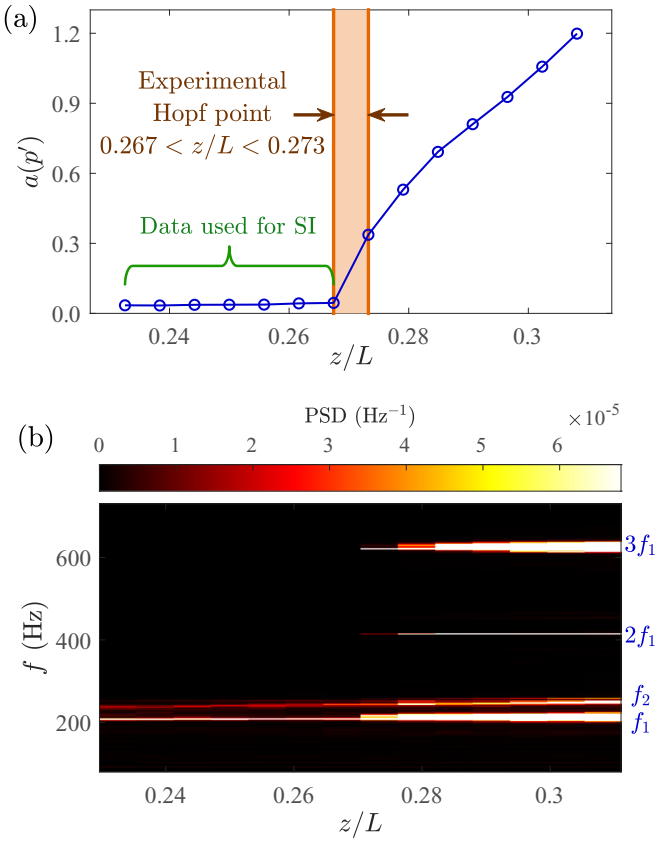


FIG. 5. (a) Experimental bifurcation diagram of the system, where the horizontal axis is the normalized flame position ($z/L$) measured from the top of the combustor. Also shown is (b) the PSD of the pressure fluctuations as a function of $z/L$.

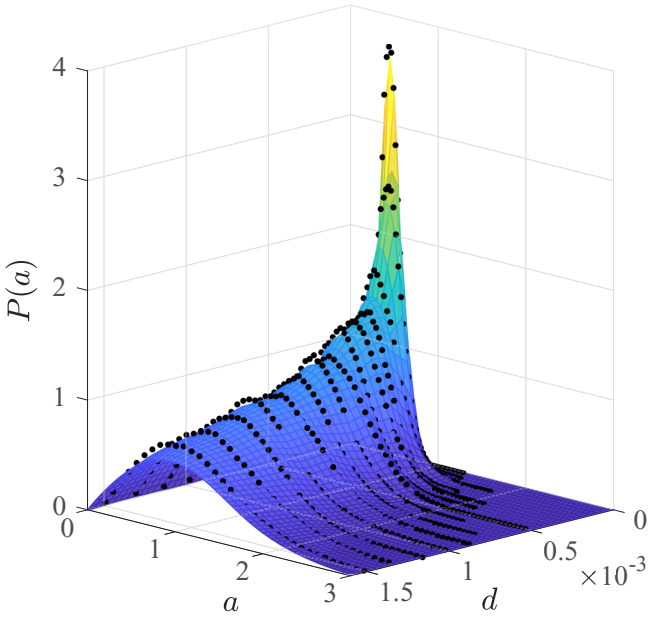


FIG. 6. Experimental probability density function (black dots) and its surface interpolation on the fixed-point branch ($z/L = 0.267$), just before the Hopf point. For all the noise amplitudes tested, $P(a)$ is unimodal, confirming the supercritical nature of the Hopf bifurcation.

and $b$ are determined by linear regression, as per Fig. 3(b). In this way, we determine the relationship between $d$ and $V$ to be $d = (2.345 \times 10^{-2})V^{1.919}$. In our experiments, the background noise amplitude ($b$) is negligible, as evidenced by the zero vertical intercept of the data shown in Fig. 3(b).

## IV. RESULTS AND DISCUSSION

Figure 5(a) shows a bifurcation diagram of the system. When the flame reaches a position of $0.267 < z/L < 0.273$, the system transitions from a fixed point to a limit cycle via a supercritical Hopf bifurcation. The supercritical nature of this bifurcation can be confirmed by examining the probability density function $P(a)$. If $P(a)$ shows two local maxima with respect to $a$ at intermediate noise amplitudes $d$ (a feature called bimodality [57]), then the system is undergoing a subcritical Hopf bifurcation. However, if $P(a)$ is unimodal, exhibiting only one peak at every value of $d$, then the system is undergoing a supercritical Hopf bifurcation. Figure 6 shows $P(a)$ and its surface interpolation on the fixed-point branch ($z/L = 0.267$), just before the Hopf point. There is only one peak for every value of $d$, confirming that the Hopf bifurcation is indeed supercritical.

Figure 5(b) shows the PSD as a function of the flame position ($z/L$). Before the Hopf point ($z/L < 0.267$), the PSD contains mostly broadband noise, with slight increases around 200–250 Hz due to incipient modes. Just after the Hopf point ($0.273 < z/L < 0.285$), the PSD is dominated by sharp peaks at $f_1 = 208$ Hz and its higher harmonics, indicating a limit cycle. Accompanying this primary mode is a weaker secondary mode at $f_2 = 243$ Hz. This secondary mode, however, is more than 100 times weaker than the primary mode, so the system dynamics is still dominated by the limit cycle at $f_1$. Further from the Hopf point ($z/L > 0.285$), the secondary mode ($f_2$) remains relatively unchanged, but the primary mode ($f_1$) and its higher harmonics ($2f_1$ and $3f_1$) continue to grow. This is particularly true for the third harmonic ($3f_1$), which grows to nearly the same amplitude as the fundamental itself ($f_1$). As we will see later, the growth of these higher harmonics has a significant influence on the limit-cycle amplitude.

The DVDP coefficients found via SI are shown in Fig. 7. The highest nonlinear term of Eq. (2) is $(\alpha_3 x^6)\dot{x}$, and the signs of the nonlinear coefficients ($\alpha_1$, $\alpha_2$, $\alpha_3$) remain unchanged across the entire range of $z/L$.

To predict the Hopf point and the resultant limit cycle using data from only the fixed-point branch, we build a mathematical relationship between $z/L$ and the system coefficients. In a Hopf bifurcation, the linear coefficient $\epsilon$ is known to be linearly proportional to the control parameter [59]. We therefore linearly extrapolate $\epsilon$ from within the fixed-point branch (i.e., from the smallest $z/L$ to the largest $z/L$ with negative $\epsilon$) to the limit-cycle branch. For the nonlinear coefficients ($\alpha_1$, $\alpha_2$, $\alpha_3$), we repeat this process but with a power law, $\alpha_n = (z/L - m_1)^{m_2}$, as per our previous study [48]. Figure 7 shows that the absolute values of the nonlinear coefficients ($|\alpha_1|$, $|\alpha_2|$, $|\alpha_3|$) decrease with increasing $z/L$. In particular, the higher the order of the nonlinear coefficients, the faster they decay, confirming that the system is indeed weakly nonlinear near the Hopf point.

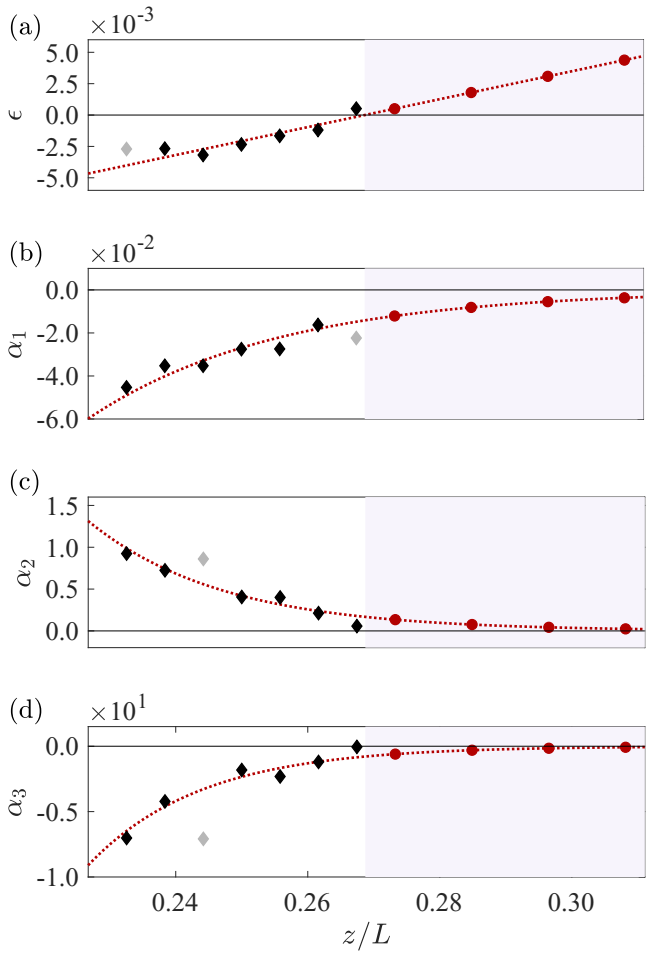


FIG. 7. Determining the DVDP coefficients via SI. Extrapolation is performed using data from only the fixed-point branch (black diamonds), after the removal of outliers (gray diamonds), which are defined here as being outside three standard deviations. The extrapolation is performed with a linear model for the linear coefficient ($\epsilon$) and with a power-law model for the nonlinear coefficients ($\alpha_1$, $\alpha_2$, $\alpha_3$). The predicted data (red circles) are on the limit-cycle branch, whose features are examined in Fig. 10.

Next we reconstruct the bifurcation diagram by solving the Stuart-Landau equation [Eq. (4)] with the extrapolated coefficients, as shown in Fig. 8. The numerical model found via SI predicts that a supercritical Hopf bifurcation occurs at $z/L = 0.269$, which agrees well with the experimentally observed Hopf point at $0.267 < z/L < 0.273$. After the Hopf point, however, the numerical predictions agree less well with the experimental data. As alluded to earlier, we speculate that this is due to the growth of the higher harmonics ($2f_1$ and $3f_1$) with increasing $z/L$. To test this, we bandpass filter the experimental limit-cycle data using different filter widths. We find improved agreement only when the higher harmonics ($2f_1$ and $3f_1$) are removed (Fig. 8); no significant difference is found when only the secondary mode ($f_2$) is removed (not shown here for brevity). The improved agreement occurs far from the Hopf point ($z/L > 0.285$), which is consistent with where the harmonics are strongest. The agreement close to the Hopf point ($z/L < 0.285$), however, remains relatively unaffected

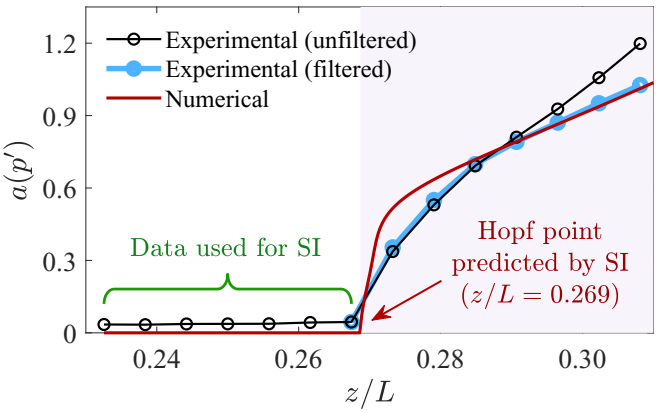


FIG. 8. Comparison of bifurcation diagrams between the experimental system and the numerical model found via SI. The Hopf point predicted by the model is at $z/L = 0.269$, which is within the experimentally observed range: $0.267 < z/L < 0.273$. The blue line represents the experimental data bandpass filtered around the limit-cycle frequency ($f_1 \pm 10$ Hz).

by the filtering, with the numerical model overpredicting the experimental data (both unfiltered and filtered; Fig. 8). This overprediction could be due to nonlinear interactions between the harmonics, which the Stuart-Landau equation [Eq. (4)] cannot capture because it was derived on the basis of weak nonlinearity (Sec. III A). In the experiments, there is substantial energy transfer from the fundamental mode ($f_1$)

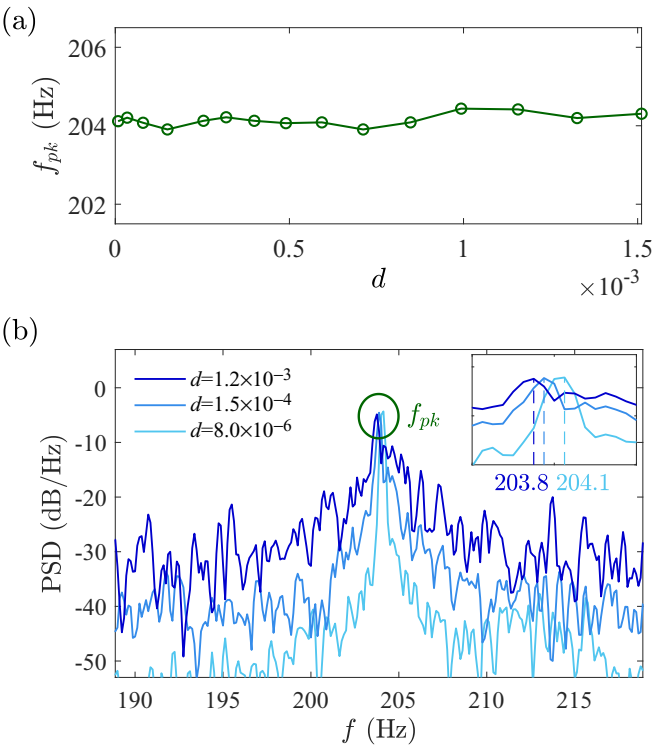


FIG. 9. Anisochronicity of the experimental system: (a) peak frequency $f_{pk}$ as a function of the noise amplitude $d$ and (b) power spectral density at different values of $d$ on the fixed-point branch ($z/L = 0.267$), just before the Hopf point. The frequency shift is observed to be less than 0.3%.

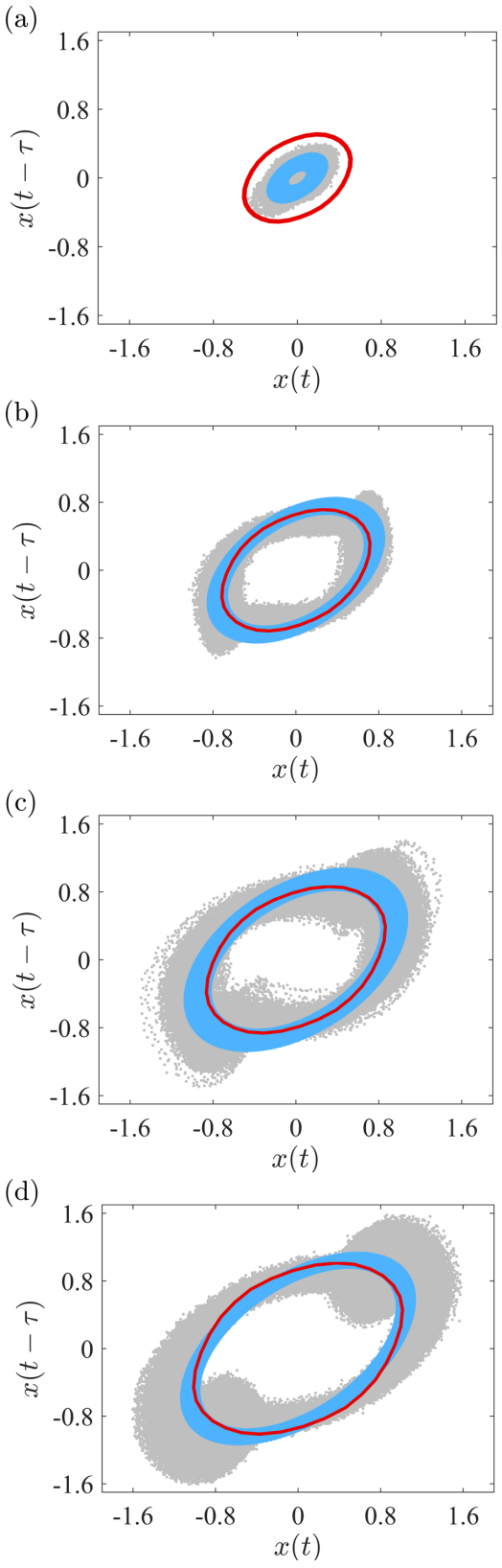


FIG. 10. Comparison of phase portraits between the experimental system and the numerical model found via SI at four different positions on the limit-cycle branch: $z/L = 0.273$ (a), 0.285 (b), 0.297 (c), and 0.308 (d). The experimental data are shown both in unfiltered form (gray) and in bandpass-filtered form (blue: $f_1 \pm 10$ Hz), while the numerical data are shown in unfiltered form only (red).

to its higher harmonics ($2f_1$ and $3f_1$). The absence of such energy transfer in the model may explain why it overpredicts the experimental data in this regime ($0.273 < z/L < 0.285$). Overall these findings show that, although the presence of strong harmonics affects the limit-cycle predictions, it does not affect the Hopf-point predictions.

To determine $\beta$ in Eq. (2), we analyze the anisochronicity of the experimental system in the frequency domain. Figure 9 shows that the dominant frequency ($f_{pk}$) shifts by less than 0.3% as $d$ increases, supporting our original assumption of a negligible frequency shift.

Finally, we examine the limit-cycle features of the numerical model using the time-delay embedding technique of Takens [60]. This technique, which has seen widespread use in thermoacoustics [61–64], enables an attractor to be reconstructed in phase space using just a single scalar time series shifted by an appropriate time delay ($\tau$). A typical choice of $\tau$ is the first minimum of the average mutual information function [65]. Figure 10 compares the phase portraits of the experimental system (both unfiltered and bandpass-filtered signals) with those of the numerical model found via SI. Owing to the presence of higher harmonics ($2f_1$ and $3f_1$), the unfiltered experimental data are seen to develop "circular swelling" as $z/L$ increases (Fig. 10). Our SI framework, however, cannot predict this feature because it assumes weak nonlinearity and hence weak harmonics. Nevertheless, if the primary mode is isolated via bandpass filtering around its fundamental frequency ($f_1 \pm 10$ Hz), the agreement between the experimental and numerical data improves far from the Hopf point [Figs. 10(b)–10(d): $z/L \geqslant 0.285$], although it remains relatively unchanged close to the Hopf point [Fig. 10(a): $z/L = 0.273$]. These trends are consistent with our discussion of Fig. 8.

## V. CONCLUSIONS

We have presented a framework for performing input-output SI near a Hopf bifurcation using data from only the fixed-point branch, prior to the Hopf point itself. The framework models the system with a DVDP-type equation perturbed by additive noise and identifies the system parameters via the corresponding Fokker-Planck equation. We have demonstrated the framework on a prototypical thermoacoustic oscillator (a flame-driven Rijke tube) undergoing a supercritical Hopf bifurcation. We find that the properties of the Hopf bifurcation—such as its location and its super- or subcritical nature—can be accurately predicted even before the onset of limit-cycle oscillations. We believe that input-output SI has been successfully performed on a reacting flow using only prebifurcation data, paving the way for the development of early warning indicators of thermoacoustic instability in combustion devices.

Compared with existing early warning indicators used in thermoacoustics, the SI framework presented here has two advantages: (i) it can predict the properties of a Hopf bifurcation without the need to set *ad hoc* instability thresholds and (ii) it can predict postbifurcation behavior such as limit-cycle amplitudes. Although demonstrated here on a thermoacoustic system, this SI framework should be applicable to other nonlinear dynamical systems as well, provided that they obey the

normal-form equation for a Hopf bifurcation (i.e., the Stuart-Landau equation). Examples of such systems include open shear flows [59], chemical reactions [66], and optical lasers [67]—among many other systems in nature and engineering.

This SI framework has two notable limitations. First, it assumes that the background noise amplitude is low. This assumption, however, may not be valid in turbulent systems, which could complicate the development of an accurate actuator model. Output-only SI methods can offer a way out of this, but they typically require large data sets, which could be difficult to acquire in practical systems [68]. Nevertheless, this problem can be circumvented with the use of adjoint equations, as Boujo and Noiray [40] have shown. Second, our SI framework makes use of time-series data collected at a single location. This works well for the thermoacoustic system studied here because its temporal dynamics is globally synchronized at every location in the flow domain. Such localized sampling keeps the matrix sizes manageable without compromising the accuracy of the numerical predictions. Other systems, however, may show elaborate spatial variations in their dynamics, requiring data to be sampled at multiple locations. In such a scenario, it may be necessary to use sparsity-promoting techniques and machine learning to process the larger data matrices [45].

## ACKNOWLEDGMENTS

This work was supported by the Research Grants Council of Hong Kong (Projects No. 16235716, No. 26202815, and No. 16210418). V.G. was supported by the National Natural Science Foundation of China (Grants No. 11672123 and No. 91752201) and the Shenzhen Science and Technology Program (Grant No. JCYJ20170412151759222).

[1] S. H. Strogatz, *Nonlinear Dynamics and Chaos: With Applications to Physics, Biology, Chemistry, and Engineering* (Westview Press, Boulder, CO, 2000).

[2] M. Abel, K. Ahnert, and S. Bergweiler, Synchronization of Sound Sources, Phys. Rev. Lett. **103**, 114301 (2009).

[3] C. Huygens, *The Pendulum Clock* (Trans RJ Blackwell, London, 1986).

[4] A. Putnam, F. Belles, and J. Kentfield, Pulse combustion, Prog. Energy Combust. Sci. **12**, 43 (1986).

[5] R. Blevins and R. Scanlan, *Flow-induced Vibration* (American Society of Mechanical Engineers Digital Collection, 1977).

[6] T. Yoshida, L. Jones, S. Ellner, G. Fussmann, and N. Hairston, Jr., Rapid evolution drives ecological dynamics in a predator–prey system, Nature (London) **424**, 303 (2003).

[7] T. Lieuwen and V. Yang, *Combustion Instabilities in Gas Turbine Engines: Operational Experience, Fundamental Mechanisms and Modeling* (AIAA, Reston, 2005).

[8] J. M. T. Thompson and H. B. Stewart, *Nonlinear Dynamics and Chaos* (John Wiley & Sons, New York, 2002).

[9] F. E. C. Culick, *Unsteady Motions in Combustion Chambers for Propulsion Systems*, AGARDograph RTO-AG-AVT-039 (NATO Research and Technology Organization, 2006).

[10] T. Poinsot, Prediction and control of combustion instabilities in real engines, P. Combust. Inst. **36**, 1 (2017).

[11] S. Candel, Combustion dynamics and control: Progress and challenges, P. Combust. Inst. **29**, 1 (2002).

[12] L. Rayleigh, The explanation of certain acoustical phenomena, Nature (London) **18**, 319 (1878).

[13] T. Lieuwen, *Unsteady Combustor Physics* (Cambridge University Press, Cambridge, UK, 2012).

[14] Y. Guan, L. K. B. Li, B. Ahn, and K. T. Kim, Chaos, synchronization, and desynchronization in a liquid-fueled diffusion-flame combustor with an intrinsic hydrodynamic mode, Chaos **29**, 053124 (2019).

[15] M. P. Juniper and R. I. Sujith, Sensitivity and nonlinearity of thermoacoustic oscillations, Annu. Rev. Fluid Mech. **50**, 661 (2018).

[16] P. G. Drazin and W. H. Reid, *Hydrodynamic Stability* (Cambridge University Press, Cambridge, UK, 2004).

[17] D. Sipp and A. Lebedev, Global stability of base and mean flows: A general approach and its applications to cylinder and open cavity flows, J. Fluid Mech. **593**, 333 (2007).

[18] L. K. B. Li and M. P. Juniper, Lock-in and quasiperiodicity in a forced hydrodynamically self-excited jet, J. Fluid Mech. **726**, 624 (2013).

[19] L. K. B. Li and M. P. Juniper, Phase trapping and slipping in a forced hydrodynamically self-excited jet, J. Fluid Mech. **735**, 1 (2013).

[20] Y. Zhu, V. Gupta, and L. K. B. Li, Onset of global instability in low-density jets, J. Fluid Mech. **828**, R1 (2017).

[21] Y. Zhu, V. Gupta, and L. K. B. Li, Coherence resonance in low-density jets, J. Fluid Mech. **881**, R1 (2019).

[22] P. Subramanian, R. I. Sujith, and P. Wahi, Subcritical bifurcation and bistability in thermoacoustic systems, J. Fluid Mech. **715**, 210 (2013).

[23] S. Etikyala and R. I. Sujith, Change of criticality in a prototypical thermoacoustic system, Chaos **27**, 023106 (2017).

[24] A. Orchini, G. Rigas, and M. P. Juniper, Weakly nonlinear analysis of thermoacoustic bifurcations in the rijke tube, J. Fluid Mech. **805**, 523 (2016).

[25] A. P. Dowling and Y. Mahmoudi, Combustion noise, P. Combust. Inst. **35**, 65 (2015).

[26] T. Lieuwen and A. Banaszuk, Background noise effects on combustor stability, J. Propul. Power **21**, 25 (2005).

[27] E. A. Gopalakrishnan and R. I. Sujith, Effect of external noise on the hysteresis characteristics of a thermoacoustic system, J. Fluid Mech. **776**, 334 (2015).

[28] V. S. Burnley and F. E. Culick, Influence of random excitations on acoustic instabilities in combustion chambers, AIAA J. **38**, 1403 (2000).

[29] V. Jegadeesan and R. I. Sujith, Experimental investigation of noise induced triggering in thermoacoustic systems, Proc. Combust. Inst. **34**, 3175 (2013).

[30] L. Kabiraj, R. Steinert, A. Saurabh, and C. O. Paschereit, Coherence resonance in a thermoacoustic system, Phys. Rev. E **92**, 042909 (2015).

[31] X. Li, D. Zhao, and B. Shi, Coherence resonance and stochastic bifurcation behaviors of simplified standing-wave thermoacoustic systems, J. Acoust. Soc. Am. **145**, 692 (2019).

[32] V. Nair and R. I. Sujith, Multifractality in combustion noise: Predicting an impending combustion instability, J. Fluid Mech. **747**, 635 (2014).

[33] T. Kobayashi, S. Murayama, T. Hachijo, and H. Gotoda, Early Detection of Thermoacoustic Combustion Instability Using a Methodology Combining Complex Networks and Machine Learning, Phys. Rev. Appl. **11**, 064034 (2019).

[34] T. Hashimoto, H. Shibuya, H. Gotoda, Y. Ohmichi, and S. Matsuyama, Spatiotemporal dynamics and early detection of thermoacoustic combustion instability in a model rocket combustor, Phys. Rev. E **99**, 032208 (2019).

[35] S. Murayama, H. Kinugawa, I. T. Tokuda, and H. Gotoda, Characterization and detection of thermoacoustic combustion oscillations based on statistical complexity and complex-network theory, Phys. Rev. E **97**, 022223 (2018).

[36] E. A. Gopalakrishnan, Y. Sharma, T. John, P. S. Dutta, and R. I. Sujith, Early warning signals for critical transitions in a thermoacoustic system, Sci. Rep. **6**, 35310 (2016).

[37] V. Gupta, A. Saurabh, C. O. Paschereit, and L. Kabiraj, Numerical results on noise-induced dynamics in the subthreshold regime for thermoacoustic systems, J. Sound Vib. **390**, 55 (2017).

[38] N. Noiray and B. Schuermans, Deterministic quantities characterizing noise driven Hopf bifurcations in gas turbine combustors, Int. J. Non-Linear Mech. **50**, 152 (2013).

[39] N. Noiray, Linear growth rate estimation from dynamics and statistics of acoustic signal envelope in turbulent combustors, J. Eng. Gas Turb. Power **139**, 041503 (2017).

[40] E. Boujo and N. Noiray, Robust identification of harmonic oscillator parameters using the adjoint Fokker–Planck equation, Proc. R. Soc. A **473**, 20160894 (2017).

[41] N. Noiray and A. Denisov, A method to identify thermoacoustic growth rates in combustion chambers from dynamic pressure time series, P. Combust. Inst. **36**, 3843 (2017).

[42] H. Risken, *Fokker–Planck Equation* (Springer, Berlin, 1984).

[43] D. T. Harrje and F. H. Reardon, Liquid propellant rocket combustion instability, Tech. Rep. No. NASA-SP-194, NASA, 1972 (unpublished).

[44] M. Schmidt and H. Lipson, Distilling free-form natural laws from experimental data, Science **324**, 81 (2009).

[45] S. L. Brunton, J. L. Proctor, and J. N. Kutz, Discovering governing equations from data by sparse identification of nonlinear dynamical systems, Proc. Natl. Acad. Sci. USA **113**, 3932 (2016).

[46] S. Jaensch, T. Emmert, C. F. Silva, and W. Polifke, A grey-box identification approach for thermoacoustic network models, *ASME Turbo Expo* (ASME Digital Collection, 2014).

[47] W. Polifke, System identification for aero-and thermo-acoustic applications, *Advances in Aero-Acoustics and Thermo-Acoustics* (von Karman Institute for Fluid Dynamics, Brussels, 2010).

[48] M. Lee, Y. Zhu, L. K. B. Li, and V. Gupta, System identification of a low-density jet via its noise-induced dynamics, J. Fluid Mech. **862**, 200 (2019).

[49] Y. Guan, M. Murugesan, and L. K. B. Li, Strange nonchaotic and chaotic attractors in a self-excited thermoacoustic oscillator subjected to external periodic forcing, Chaos **28**, 093109 (2018).

[50] Y. Guan, W. He, M. Murugesan, Q. Li, P. Liu, and L. K. B. Li, Control of self-excited thermoacoustic oscillations using transient forcing, hysteresis and mode switching, Combust. Flame **202**, 262 (2019).

[51] Y. Guan, V. Gupta, K. Kashinath, and L. K. B. Li, Open-loop control of periodic thermoacoustic oscillations: Experiments and low-order modeling in a synchronization framework, Proc. Combust. Inst. **37**, 5315 (2019).

[52] Y. Guan, V. Gupta, M. Wan, and L. K. B. Li, Forced synchronization of quasiperiodic oscillations in a thermoacoustic system, J. Fluid Mech. **879**, 390 (2019).

[53] A. H. Nayfeh, *Introduction to Perturbation Techniques* (John Wiley, New York, 1981).

[54] J.-M. Chomaz, Global instabilities in spatially developing flows: Non-normality and nonlinearity, Annu. Rev. Fluid Mech. **37**, 357 (2005).

[55] L. K. B. Li and M. P. Juniper, Lock-in and quasiperiodicity in hydrodynamically self-excited flames: Experiments and modelling, P. Combust. Inst. **34**, 947 (2013).

[56] R. L. Stratonovich, *Topics in the Theory of Random Noise* (Gordon and Breach, New York, 1963).

[57] A. Zakharova, T. Vadivasova, V. Anishchenko, A. Koseska, and J. Kurths, Stochastic bifurcations and coherencelike resonance in a self-sustained bistable noisy oscillator, Phys. Rev. E **81**, 011106 (2010).

[58] O. V. Ushakov, H. J. Wünsche, F. Henneberger, I. A. Khovanov, L. Schimansky-Geier, and M. A. Zaks, Coherence Resonance Near a Hopf Bifurcation, Phys. Rev. Lett. **95**, 123903 (2005).

[59] M. Provansal, C. Mathis, and L. Boyer, Bérnard-von Kármán instability: Transient and forced regimes, J. Fluid Mech. **182**, 1 (1987).

[60] F. Takens, Detecting strange attractors in turbulence, Lect. Notes Math. **898**, 366 (1981).

[61] S. Balusamy, L. K. B. Li, Z. Han, M. P. Juniper, and S. Hochgreb, Nonlinear dynamics of a self-excited thermoacoustic system subjected to acoustic forcing, P. Combust. Inst. **35**, 3229 (2015).

[62] C. Y. Lee, L. K. B. Li, M. P. Juniper, and R. S. Cant, Nonlinear hydrodynamic and thermoacoustic oscillations of a bluff-body stabilised turbulent premixed flame, Combust. Theor. Model. **20**, 131 (2016).

[63] K. Kashinath, L. K. B. Li, and M. P. Juniper, Forced synchronization of periodic and aperiodic thermoacoustic oscillations: Lock-in, bifurcations and open-loop control, J. Fluid Mech. **838**, 690 (2018).

[64] Y. Guan, P. Liu, B. Jin, V. Gupta, and L. K. B. Li, Nonlinear time-series analysis of thermoacoustic oscillations in a solid rocket motor, Exp. Therm. Fluid Sci. **98**, 217 (2018).

[65] A. M. Fraser and H. L. Swinney, Independent coordinates for strange attractors from mutual information, Phys. Rev. A **33**, 1134 (1986).

[66] Y. Kuramoto, *Chemical Oscillations, Waves, and Turbulence* (Courier Corporation, New York, 2003).

[67] K. Lüdge and H. Schuster, *Nonlinear Laser Dynamics: From Quantum Dots to Cryptography* (John Wiley & Sons, New York, 2012), Vol. 5.

[68] L. Mevel, A. Benveniste, M. Basseville, M. Goursat, B. Peeters, H. Van der Auweraer, and A. Vecchio, Input/output versus output-only data processing for structural identification–Application to in-flight data analysis, J. Sound Vib. **295**, 531 (2006).